

## Scaled propagation invariant Bessel beams

F. Soto-Eguibar<sup>a</sup>, I. Ramos-Prieto<sup>a</sup>, D. Sánchez-de-la-Llave<sup>a</sup>, U. Ruíz<sup>a</sup>,  
J. A. Anaya-Contreras<sup>b</sup>, A. Zúñiga-Segundo<sup>b</sup>, and H. M. Moya-Cessa<sup>a</sup>

<sup>a</sup>*Instituto Nacional de Astrofísica Óptica y Electrónica,  
Calle Luis Enrique Erro 1, Santa María Tonantzintla, Puebla, 72840, México.*

<sup>b</sup>*Instituto Politécnico Nacional, ESFM, Departamento de Física,  
Edificio 9, Unidad Profesional Adolfo López Mateos, 07738 CDMX., México.*

Received 18 March 2024; accepted 27 January 2025

We present a new family of Bessel solutions of the paraxial equation. Such solutions keep their form during propagation because of a quadratic phase factor that makes them scaled propagation invariant fields. When a Gaussian support is incorporated, the solution loses its invariant properties, although, over some volume, it closely resembles a scaled propagation invariant field. The Bessel beams we introduce have the particularity that they present a very strong focusing effect and do not necessarily require a Gaussian support.

*Keywords:* Bessel; Gaussian.

DOI: <https://doi.org/10.31349/RevMexFis.71.041301>

### 1. Introduction

Novel closed-form solutions to the paraxial equation in cylindrical coordinates have been proposed over the last 40 years. In a seminal paper, Durning presented in 1987 [1] an exact solution to the scalar wave equation, namely the zero-order Bessel function of the first kind, which has the property of maintaining its intensity pattern in any transverse plane, *i.e.* a non-diffracting beam, opening up a very prolific research area. Among its more relevant applications, we can mention particle trapping and energy transfer through the orbital angular momentum of light. Shortly after, Gori *et al.* [2] found an exact solution that consisted of multiplying the Bessel function  $J_0$  by a Gaussian distribution, calling this solution the Bessel-Gauss beam of zero order. A clear advantage of the latter solution is that it possesses finite energy at any transverse plane, making it physically realizable, although the non-diffracting properties are also affected. Some years later, Caron *et al.* [3] (see also [4]) presented an exact solution to the paraxial equation consisting of a Gaussian function multiplied by a Bessel function with quadratic radial dependence and a quadratic phase function; the proposed solution also includes a topological charge that doubles the order of the Bessel function, and its transverse intensity profile has most of its energy concentrated in a single ring. Later, Cai *et al.* [5] presented a solution consisting of a Gaussian function multiplied by the radial coordinate elevated to an even power, producing a transverse intensity consisting of a single ring carrying all the beam energy; this solution was called a hollow Gaussian beam. In 2007 [6, 7], a broad family of closed-form solutions to the paraxial equation was introduced, called hypergeometric and hypergeometric-Gaussian beams, the latter having as a particular case the solutions reported in [3]. One year later, Kotlyar *et al.* reported another family of hypergeometric beams [8], while Bandres *et al.* reported circular beams [9], the most general closed-form solution to the

paraxial equation in circular cylindrical coordinates reported so far.

We present a novel family of closed-form solutions to the paraxial equation in cylindrical coordinates. Our approach consists of proposing an ansatz that contains a Gaussian distribution multiplied by a Bessel function of the first kind with quadratic radial dependence and a topological charge that doubles the order of the Bessel function. In addition, the amplitude is modulated by a function that varies with the propagation distance. First, we show a family of solutions with infinite energy in any transverse plane to the  $z$ -axis. Subsequently, a Gaussian function is introduced employing quantum optic operators, resulting in an additional set of solutions characterized by finite energy along any transverse plane to the  $z$ -axis.

These new solutions exhibit a focusing effect, which is a remarkable characteristic in the field of wave optics. This effect allows the solutions to concentrate the majority of their energy within a single, sharply defined ring. Such a configuration is particularly advantageous for applications that require high-intensity focal points, as it ensures that energy is not dispersed but rather confined to a specified region in space. This confinement not only enhances the beam's intensity but also improves the precision and efficacy of its interaction with materials or particles. The ability of these beams to maintain their structural integrity during propagation is attributed to the designed quadratic phase factor. This phase factor acts as a stabilizing mechanism, allowing the beam to preserve its form and energy distribution over certain distances. The quadratic dependence ensures that as the beam propagates, it dynamically adjusts its phase, compensating for potential diffraction effects that would normally lead to beam spreading. The stability and resilience offered by this quadratic phase factor make these beams suitable for applications that demand long-range propagation without loss of

beam quality. In practical terms, this means that the beams can be employed in environments where maintaining a consistent and focused energy delivery is critical, such as in optical tweezers for precise particle manipulation, in advanced imaging systems where clarity and focus are paramount, and in telecommunications where signal integrity over distance is essential. Furthermore, the robustness of these beams against diffraction and their energy-efficient design open new avenues for exploration in fields ranging from biomedical engineering, where they can enhance the precision of laser surgery, to material science, where focused energy delivery can facilitate advanced fabrication techniques. The combination of a pronounced focusing effect with propagation invariance thus represents a significant leap forward in the capabilities of optical beam technologies.

This approach is motivated by acknowledging the similarity between the paraxial wave equation and the Schrödinger equation in quantum theory [10]. Notably, the temporal variable in the Schrödinger equation corresponds to the coordinate along the propagation axis in the paraxial wave equation, establishing a formal analogy that is widely understood and linking wave optics and quantum mechanics. The solutions we present hereafter can not be obtained from the general solutions proposed in the past, and they distinguished themselves from the ones proposed in Ref. [3] by the strong focusing effect they possess. We believe that the solutions can be of interest to applications in several fields. All beams proposed and analyzed in this work were produced and tested experimentally, as explained in Sec. 4. In Figs. 3 and 4 the experimental results are presented, together with the theoretical predictions.

## 2. Ansatz for a simple solution

A method for finding solutions to the wave equation is the ansatz method, which involves proposing a solution composed of the product of two guessed functions. In this context, we are seeking solutions of the form

$$E_\mu(r, \theta, z) = \frac{1}{\sqrt{z}} \exp\left(i \frac{kr^2}{4z}\right) J_\mu\left(\frac{kr^2}{4z}\right) \exp(2i\mu\theta). \quad (1)$$

This field satisfies the paraxial equation

$$\nabla_\perp^2 E(r, \theta, z) + 2ik \frac{\partial E(r, \theta, z)}{\partial z} = 0, \quad (2)$$

in cylindrical coordinates. The validity of this solution can be easily verified by a simple direct substitution (for more details, see Appendix A). As can be observed, Eq. (1) represents a field that changes its scale as it propagates, or, in other words, a propagation-invariant field on a scale. For the field to have real physical significance, the parameter  $k$  must be real and, without loss of generality, considered strictly positive. Additionally, the parameter  $\mu$  must be an integer or a semi-integer, which can be taken, again without loss of generality, as equal to or greater than zero.

Figure 1 exemplifies the scaled propagation invariant attribute of this field across planes at  $z = 0.10$  m,  $z = 0.25$  m, and  $z = 0.50$  m. Figure 1a) presents the intensity distribution of the field as a function of  $r$  for the three distinct propagation distances, while Figs. 1b), 1c), and 1d) depict the field intensity across three transverse planes at the same propagation distances.

## 3. Providing a Gaussian support

The field described by Eq. (1) is not square-integrable, akin to typical Bessel beams. Similarly to other diffractive beams, such as Bessel beams [1], these solutions lack physical realizability due to their non-square integrable nature. To overcome this constraint, drawing insight from the Bessel-Gauss beams [2], we aim to develop a generalized variant incorporating a Gaussian factor, ensuring that the field becomes square-integrable. Consequently, our quest involves crafting a generalized version incorporating a multiplicative Gaussian factor to render it square-integrable. To achieve this goal, we write the paraxial equation as a Schrödinger-like equation,

$$\frac{\partial E(x, y, z)}{\partial z} = \frac{i}{2k} \nabla_\perp^2 E(x, y, z), \quad (3)$$

whose formal solution is

$$E(x, y, z) = \exp\left(\frac{i}{2k} z \nabla_\perp^2\right) E(x, y, 0), \quad (4)$$

being  $E(x, y, 0)$  the initial field at  $z = 0$ . The choice to consider the paraxial equation as a Schrödinger-like equation stems from the possibility of employing an operator approach within the realm of quantum optics, an unconventional approach in paraxial optics [10, 12, 13]. Taking this into consideration in Cartesian coordinates, the aforementioned equation can be reformulated as:

$$E(x, y, z) = \exp\left[-\frac{i}{2k} z (\hat{p}_x^2 + \hat{p}_y^2)\right] E(x, y, 0), \quad (5)$$

where we introduced the operators  $\hat{p}_x = -i(\partial/\partial x)$  and  $\hat{p}_y = -i(\partial/\partial y)$ , satisfying the following commutation relations:  $[x, \hat{p}_x] = [y, \hat{p}_y] = i$  and  $[x, y] = [x, \hat{p}_y] = [y, \hat{p}_x] = [\hat{p}_x, \hat{p}_y] = 0$ . Next, we express the initial condition as

$$E(x, y, 0) = \exp[-g(x^2 + y^2)] \mathcal{E}(x, y), \quad (6)$$

with  $g$  a positive real constant, and  $\mathcal{E}(x, y)$  represents a currently generic field. Substituting this initial condition into Eq. (5), we obtain

$$E(x, y, z) = \exp\left[-\frac{i}{2k} z (\hat{p}_x^2 + \hat{p}_y^2)\right] \times \exp[-g(x^2 + y^2)] \mathcal{E}(x, y, 0). \quad (7)$$

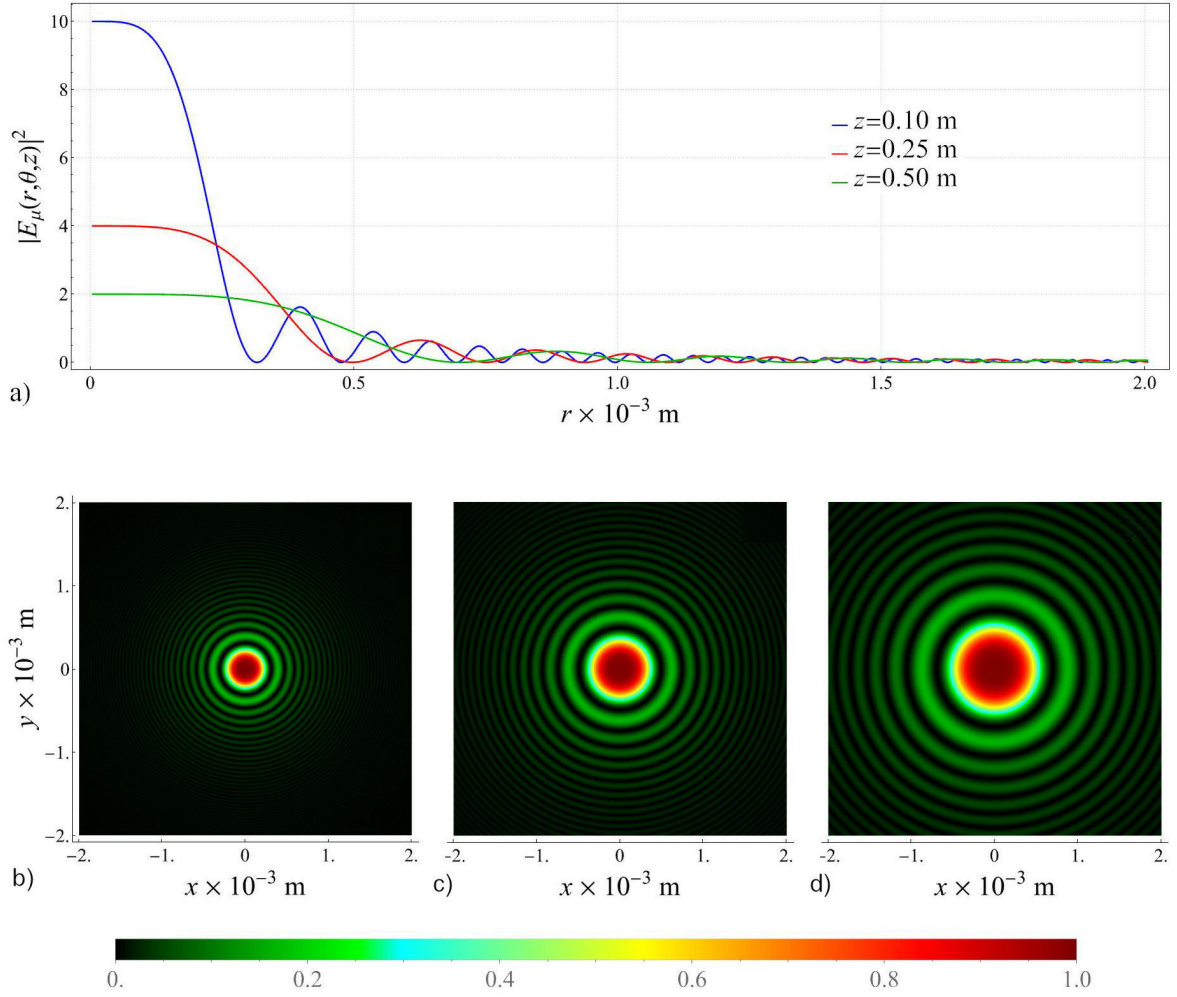


FIGURE 1. Intensity distribution of the field as determined by Eq. (1). a) Profile illustrating the intensity distribution as a function of the radius  $r$  at  $z = 0.10$  m,  $0.25$  m,  $0.50$  m. b)-(d) Field intensity distribution in three observation planes (same propagation distances as in a)) perpendicular to the propagation distance. The implemented physical parameters for the beam are  $k = 9.926 \times 10^6 \text{ m}^{-1}$  ( $\lambda = 633 \text{ nm}$ ), and  $\mu = 0$ .

Now, we introduce the identity operator  $\hat{I}$ , written as  $\hat{I} = e^{(i/2k)z(\hat{p}_x^2 + \hat{p}_y^2)} e^{-(i/2k)z(\hat{p}_x^2 + \hat{p}_y^2)}$ , before  $\mathcal{E}(x, y)$ ,

$$\begin{aligned}
 E(x, y, z) &= \exp\left[-\frac{i}{2k}z(\hat{p}_x^2 + \hat{p}_y^2)\right] \exp[-g(x^2 + y^2)] \\
 &\times \exp\left[\frac{i}{2k}z(\hat{p}_x^2 + \hat{p}_y^2)\right] \exp\left[-\frac{i}{2k}z(\hat{p}_x^2 + \hat{p}_y^2)\right] \\
 &\times \mathcal{E}(x, y). \quad (8)
 \end{aligned}$$

Hereafter, leveraging standard operator techniques of quantum optics, we transit to polar coordinates, leading to the following expression:

$$\begin{aligned}
 E(r, \theta, z) &= \frac{k}{k + 2igz} \exp(ar^2) \exp(2br\hat{p}_r) \\
 &\times \exp\left(i\frac{1}{2k} \frac{kz}{k + 2igz} \nabla_{\perp}^2\right) \mathcal{E}(r, \theta), \quad (9)
 \end{aligned}$$

where the coefficients are determined by:  $a =$

$-gk/(k + 2igz)$  and  $b = -(\pi/4) - (i/2) \ln(i - [2gz/k])$ , with  $\hat{p}_r = -i(\partial/\partial r)$ .

We establish a connection with the initial simple solution given by Eq. (1). Since the field described in Eq. (1) satisfies the paraxial equation, it requires an initial condition, denoted as  $\mathcal{E}(r, \theta)$ , from which it evolves. This evolution is expressed as

$$\begin{aligned}
 \exp\left(\frac{i}{2k} \frac{kz}{k + 2igz} \nabla_{\perp}^2\right) \mathcal{E}(r, \theta) &= \sqrt{\frac{k + 2igz}{kz}} \\
 &\times \exp\left(\frac{ir^2(k + 2igz)}{4z}\right) \\
 &\times J_{\mu}\left(\frac{r^2(k + 2igz)}{4z}\right) \exp(2i\mu\theta), \quad (10)
 \end{aligned}$$

and where  $z$ , in Eq. (1), has been substituted by  $kz/(k + 2igz)$ . What follows is laborious, but easy and direct, and leads us to the following expression:

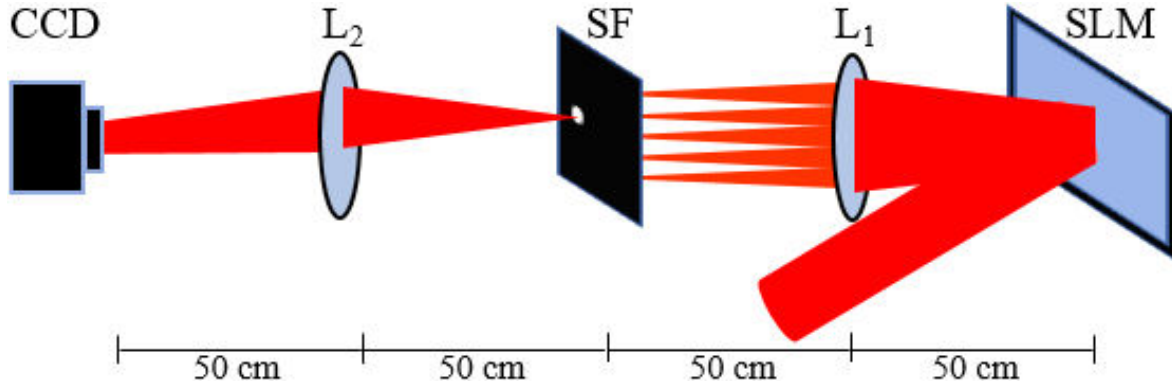


FIGURE 2. Experimental setup. Spatial light modulator (SLM), lenses ( $L_1$  and  $L_2$ ), spatial filter (SF), and CCD camera (CCD).

$$\begin{aligned}
 E_{\mu}(r, \theta, z) = & \exp(2i\mu\theta) \sqrt{\frac{k}{z(k+2igz)}} \\
 & \times \exp\left[\frac{kr^2(ik-4gz)}{4z(k+2igz)}\right] \\
 & \times J_{\mu}\left(\frac{k^2r^2}{4kz+8igz^2}\right). \quad (11)
 \end{aligned}$$

This constitutes our new exact solution to the paraxial equation, named the *scaled propagation invariant Bessel beam*. Introducing a Gaussian support disrupts the invariant nature of the field originally contained in Eq. (1), similar to how the Bessel-Gauss beam deviates from the propagation invariance of the unbounded Bessel beam. However, it is important to note that, over the propagation distances where  $4gz$  is much smaller than  $k$ , the field described by Eq. (11) maintains a scaled propagation quasi-invariance. In these conditions, the impact of the Gaussian support on the field invariance is minimized, allowing the beam to effectively preserve its structural integrity and energy distribution over significant distances. This quasi-invariance means that while the beam does not remain perfectly invariant, its deviation from ideal behavior is small enough to be negligible for many practical applications, especially those that do not require extreme long-range propagation. As a result, the propagation characteristics of these newly scaled propagation-invariant Bessel beams remain highly relevant to applications, offering a practical balance between physical realizability and functional performance. This nuanced understanding of the quasi-invariant behavior helps in leveraging the benefits of the Gaussian support while mitigating its potential drawbacks in specific scenarios.

#### 4. Experimental setup and results

We generate some fields experimentally, in order to show good agreement with the theoretical ones. For this task, we use a synthetic phase hologram capable of encoding any complex field,  $s(x, y) = a(x, y) \exp[i\phi(x, y)]$ , where  $a(x, y)$  and

$\phi(x, y)$  represent the amplitude and the phase modulation, respectively. The synthetic phase hologram is given by [11].

$$h(x, y) = \exp(iff[a(x, y)] \sin[\phi(x, y)]). \quad (12)$$

For instance, the function  $f[a(x, y)]$  can be evaluated through the relationship  $J_1(f[a(x, y)]) = A a(x, y)$ . The maximum value of  $A$  that satisfies Eq. (12) is  $A = 0.5819$ , corresponding to the peak value of the first-order Bessel function  $J_1(\alpha)$ , which, in turn, occurs at  $\alpha = 1.84$ . Using a  $4f$ -optical system, shown in Fig. 2, we display the corresponding synthetic phase hologram on a phase-only spatial light modulator (SLM), which is induced by a collimated He-Ne laser ( $\lambda = 633$  nm). The lens  $L_1$  performs the Fourier transform of the phase hologram at its back focal length ( $f_1$ ), a spatial filter (SF) blocks the noise-diffracted orders and the lens  $L_2$  recovers the codified complex field.

Figure 3 shows the intensity distribution of such a field in the planes  $z = 0.10$  m,  $z = 0.25$  m, and  $z = 0.50$  m. On the other hand, Fig. 4 shows the intensity distribution for planes where the field does not scale anymore as it propagates. In the latter case, the value of  $g$  is an order of magnitude greater than that used in Fig. 3. To generate the fields in both figures, we used the experimental setup shown in Fig. 2.

Finally, Fig. 5 illustrates a transverse view ( $x, y = 0$ ) displaying the field intensity between  $z = 0.0$  m and  $z = 1.0 \times 10^{-1}$  m. At  $z = 0$ , the field achieves its maximum focus, evident from its peak intensity. At the focal point of  $z = 0$ , the field exhibits its maximum concentration, as evidenced by its peak intensity. However, beyond this focal juncture a change occurs in the factor governing the field's focusing behavior, leading to an expansion in its intensity profile. It is important to note that the solution represented by Eq. (11) becomes indeterminate, as a common function, at  $z = 0$ ; for clarity, in the visualization depicted in Fig. 4 we omitted this particular plane. Interestingly, as the field approaches  $z = 0$ , its intensity diverges, resembling the behavior of a Dirac delta function, characterized by an intensity profile similar to  $1/z$ .

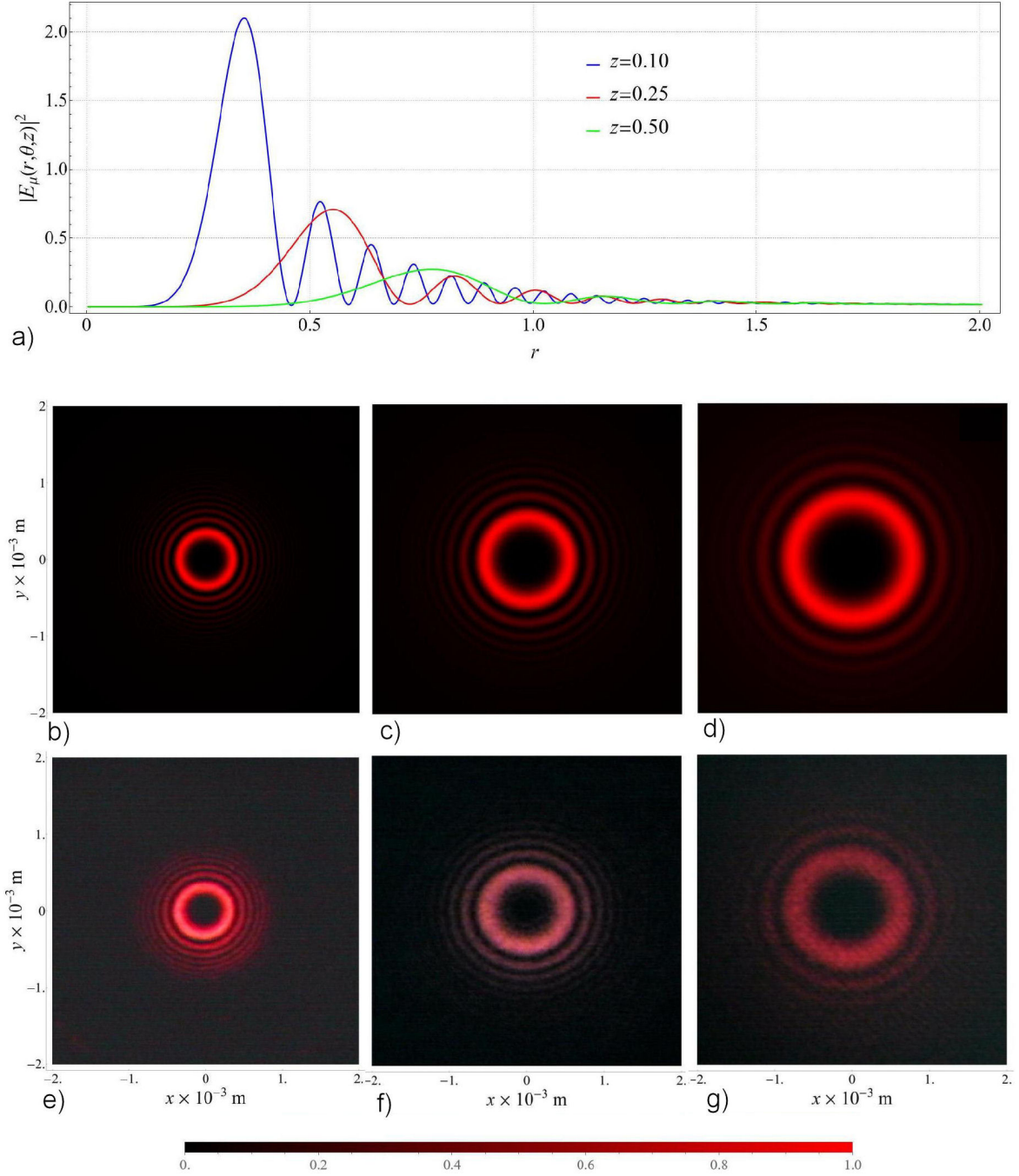


FIGURE 3. Intensity distribution of the field as determined by Eq. (11). a) Profile illustrating the intensity distribution as a function of the radius  $r$  at  $z = 0.10$  m,  $0.25$  m,  $0.50$  m. b)-d) Field intensity distribution in three observation planes (same propagation distances as in (a)) perpendicular to the propagation distance. The physical parameters of the beam are  $k = 9.926 \times 10^6 \text{ m}^{-1}$  ( $\lambda = 633 \text{ nm}$ ),  $\mu = 2$ , and  $g = (|k|/10) \text{ m}^{-2}$ . e)-g) Experimental realization using the same parameters.

## 5. The field is transversally square-integrable

We now prove that the introduced beams, Eq. (11), are square-integrable. Substituting the field intensity of the field Eq. (11) in the integral over all space and performing the integral in  $\theta$ , we get

$$\int_0^\infty r dr \int_0^{2\pi} d\theta |E(r, \theta, z)|^2 = \frac{2\pi k}{|z| \sqrt{k^2 + 4g^2 z^2}} \int_0^\infty \exp\left(-\frac{gk^2 r^2}{k^2 + 4g^2 z^2}\right) \left| J_\mu\left(\frac{k^2 r^2}{4kz + 8igz^2}\right) \right|^2 r dr. \quad (13)$$

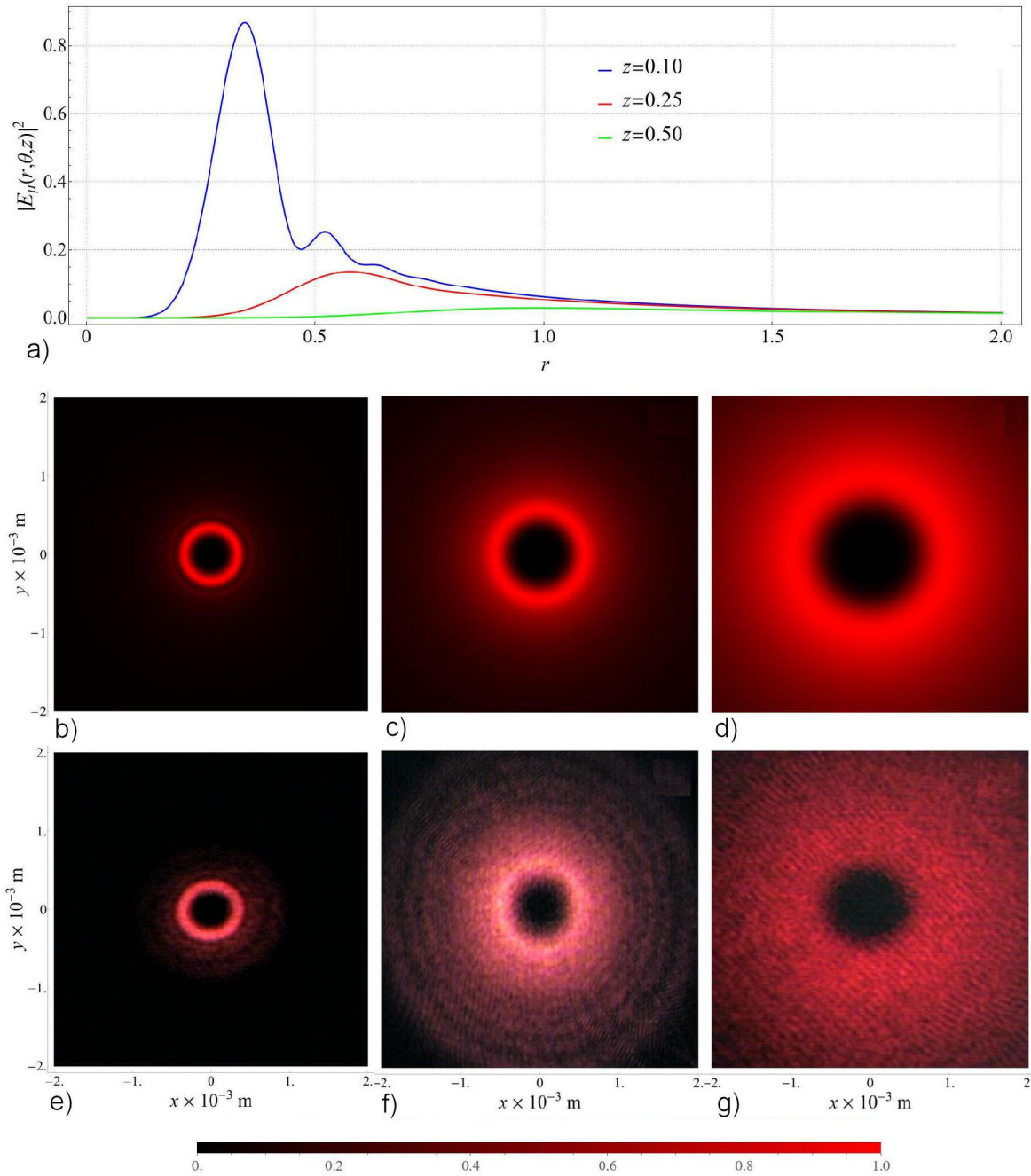


FIGURE 4. Intensity distribution of the field as determined by Eq. (11). a) Profile illustrating the intensity distribution as a function of the radius  $r$  at  $z = 0.10$  m,  $0.25$  m,  $0.50$  m. b)- d) Field intensity distribution in three observation planes (same propagation distances as in a)) perpendicular to the propagation distance. The physical parameters of the beam are  $k = 9.926 \times 10^6 \text{ m}^{-1}$  ( $\lambda = 633$  nm),  $\mu = 2$ , and  $g = |k| \text{ m}^{-2}$ . e)-g) Experimental realization using the same parameters.

We have not been able to compute the integral over  $r$ , but we can show that it is finite; to do that, we use theorem [14, 15]:

**Theorem 1.** *If  $\nu$  is real and  $\nu \geq -1/2$ ,*

$$|J_\nu(\zeta)| \leq \frac{1}{\Gamma(\nu + 1)} \left| \frac{\zeta}{2} \right|^\nu \exp[\text{Im}(\zeta)], \quad (14)$$

where  $\zeta$  is an arbitrary complex number.

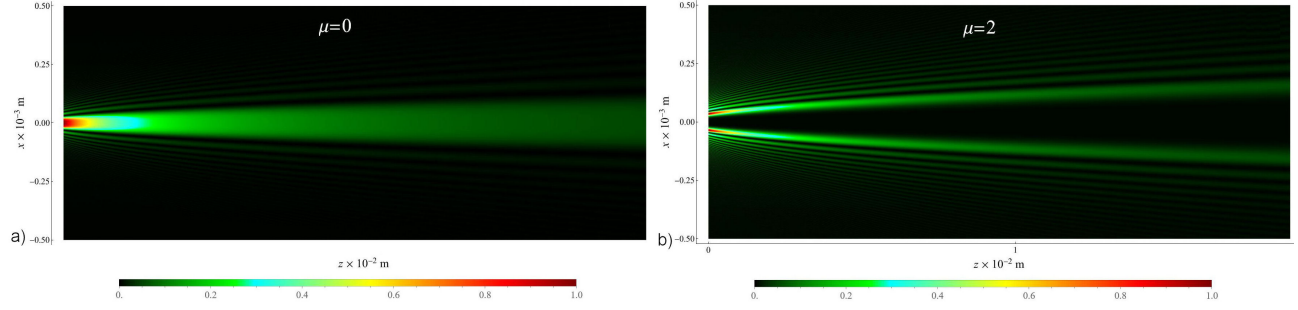


FIGURE 5. Visually depict the propagated intensity profile of the field governed by Eq. (11), for two distinct values of  $\mu$ : a)  $\mu = 0$  and b)  $\mu = 2$ . We employed the same set of physical parameters utilized in constructing Fig. 3, *i.e.*,  $k = 9.926 \times 10^6 \text{ m}^{-1}$  ( $\lambda = 633 \text{ nm}$ ) and  $g = (|k|/10) \text{ m}^{-2}$ .

Consequently, we have

$$\left| J_\mu \left( \frac{k^2 r^2}{4kz + 8igz^2} \right) \right| \leq \exp \left[ -\frac{gk^2 r^2}{2k^2 + 8g^2 z^2} \right] \frac{(kr)^{2\mu}}{8^\mu \Gamma(\mu + 1) z^\mu (4g^2 z^2 + k^2)^{\mu/2}}. \quad (15)$$

Using elementary calculus, we conclude that

$$\int_0^\infty \exp \left( -\frac{gk^2 r^2}{4g^2 z^2 + k^2} \right) \left| J_\mu \left( \frac{k^2 r^2}{4kz + 8igz^2} \right) \right|^2 r dr \leq \frac{k^{4\mu}}{64^\mu \Gamma^2(\mu + 1) z^{2\mu+1} (k^2 + 4g^2 z^2)^{\mu+1/2}} \times \int_0^\infty r^{4\mu+1} \exp \left( -\frac{2gk^2 r^2}{k^2 + 4g^2 z^2} \right) dr. \quad (16)$$

The integral on the right side of the previous inequality can be easily done, and it is finite and positive; thus, the paraxial Bessel beams, defined in Eq. (11), are square-integrable.

## 6. Conclusions

We have presented a new family of closed-form solutions of the paraxial equation, which is essentially formed by a Bessel factor with quadratic dependence in the radius. The fields are re-scaled as they propagate. We incorporate a Gaussian support into the solution employing quantum optics mathematical tools, yielding a field that is scaled propagation quasi-invariant over some propagation distance and then loses this property. A very important characteristic of the new solutions presented in this work, that differentiates them from those introduced previously [3,4], is that they are square-integrable Eq. (11), do not require Gaussian support Eq. (1), although they allow it, and the focusing is very strong. Thus, we suggest naming them as *scaled propagation invariant Bessel beams*.

The applications of these scaled propagation-invariant Bessel beams span a wide array of fields. Their inherent focusing capability makes them promising candidates for numerous practical applications, including but not limited to particle manipulation and trapping, biomedical applications, and material processing and engineering. In conclusion, the introduction of scaled propagation invariant Bessel beams represents a significant stride forward in optical field solutions that offer versatile and impactful applications across various scientific and technological domains.

## Appendix

### A. Demonstration that the ansatz field, Eq. (1), is the solution of the paraxial equation

We show that the field

$$E_\mu(r, \theta, z) = \frac{1}{\sqrt{z}} \exp(2i\mu\theta) \exp\left(i\frac{kr^2}{4z}\right) J_\mu\left(\frac{kr^2}{4z}\right), \quad (A.1)$$

is a solution of the paraxial equation

$$\nabla_\perp^2 E(r, \theta, z) + 2ik \frac{\partial E(r, \theta, z)}{\partial z} = 0, \quad (A.2)$$

in cylindrical coordinates.

To do this, we obtain the derivatives of Eq. (A.1) with respect to  $r$ ,

$$\frac{\partial E_\mu(r, \theta, z)}{\partial r} = \frac{kr}{2z^{3/2}} \exp(2i\mu\theta) \exp\left(i\frac{kr^2}{4z}\right) \left[ J'_\mu\left(\frac{kr^2}{4z}\right) + iJ_\mu\left(\frac{kr^2}{4z}\right) \right], \quad (\text{A.3})$$

and

$$\begin{aligned} \frac{\partial^2 E_\mu(r, \theta, z)}{\partial r^2} &= \frac{k}{4z^{5/2}} \exp(2i\mu\theta) \exp\left(i\frac{kr^2}{4z}\right) \\ &\times \left[ -kr^2 J''_\mu\left(\frac{kr^2}{4z}\right) - 2(ikr^2 + z) J'_\mu\left(\frac{kr^2}{4z}\right) + (kr^2 - 2iz) J_\mu\left(\frac{kr^2}{4z}\right) \right], \end{aligned} \quad (\text{A.4})$$

where the prime means derivative with respect to the argument of the function.

The second derivative with respect to  $\theta$  is

$$\frac{\partial^2 E_\mu(r, \theta, z)}{\partial \theta^2} = -\frac{4\mu^2}{\sqrt{z}} \exp(2i\mu\theta) \exp\left(i\frac{kr^2}{4z}\right) J_\mu\left(\frac{kr^2}{4z}\right). \quad (\text{A.5})$$

Thus, the two-dimensions Laplacian reads

$$\begin{aligned} \nabla_{\perp}^2 E_\mu(r, \theta, z) &= \frac{1}{4r^2 z^{5/2}} \exp(2i\mu\theta) \exp\left(i\frac{kr^2}{4z}\right) \\ &\times \left[ k^2 r^4 J''_\mu\left(\frac{kr^2}{4z}\right) + 2kr^2(ikr^2 + 2z) J'_\mu\left(\frac{kr^2}{4z}\right) + (-k^2 r^4 + 4ikr^2 z - 16\mu^2 z^2) J_\mu\left(\frac{kr^2}{4z}\right) \right]. \end{aligned} \quad (\text{A.6})$$

To complete the paraxial wave equation, we need the derivative with respect to  $z$ ,

$$\begin{aligned} 2ik \frac{\partial E_\mu(r, \theta, z)}{\partial z} &= \frac{1}{4r^2 z^{5/2}} \exp(2i\mu\theta) \exp\left(i\frac{kr^2}{4z}\right) \\ &\times \left[ k^2 r^4 J''_\mu\left(\frac{kr^2}{4z}\right) + 4kr^2 z J'_\mu\left(\frac{kr^2}{4z}\right) + (k^2 r^4 - 16\mu^2 z^2) J_\mu\left(\frac{kr^2}{4z}\right) \right]. \end{aligned} \quad (\text{A.7})$$

Hence, the paraxial equation can be cast as

$$k^2 r^4 J''_\mu\left(\frac{kr^2}{4z}\right) + 4kr^2 z J'_\mu\left(\frac{kr^2}{4z}\right) + (k^2 r^4 - 16\mu^2 z^2) J_\mu\left(\frac{kr^2}{4z}\right) = 0. \quad (\text{A.8})$$

From [16, formula 8.491.2, page 931] and [14, formula 9.1.53, page 362], we know that

$$k^2 r^4 J''_\mu\left(\frac{kr^2}{4z}\right) = -4kr^2 z J'_\mu\left(\frac{kr^2}{4z}\right) - (k^2 r^4 - 16\mu^2 z^2) J_\mu\left(\frac{kr^2}{4z}\right), \quad (\text{A.9})$$

and substituting in the paraxial equation in the form Eq. (A.8), we get that it is satisfied.

1. J. Durnin, Exact solutions for nondiffracting beams. I. The scalar theory, *J. Opt. Soc. Am. A* **4** (1987) 651, <https://doi.org/10.1364/JOSAA.4.000651>
2. F. Gori, G. Guattari, C. Padovani, Bessel-Gauss beams, *Optics Communications* **64** (1987) 491, [https://doi.org/https://doi.org/10.1016/0030-4018\(87\)90276-8](https://doi.org/https://doi.org/10.1016/0030-4018(87)90276-8)
3. C. Caron, R. Potvliege, Bessel-modulated gaussian beams with quadratic radial dependence, *Optics Communications* **164** (1999) 83, [https://doi.org/https://doi.org/10.1016/S0030-4018\(99\)00174-1](https://doi.org/https://doi.org/10.1016/S0030-4018(99)00174-1)
4. A. Belafhal, L. Dalil-Essakali, Collins formula and propagation of Bessel-modulated Gaussian light beams through an abcd optical system, *Optics Communications* **177** (2000) 181, [https://doi.org/https://doi.org/10.1016/S0030-4018\(00\)00600-3](https://doi.org/https://doi.org/10.1016/S0030-4018(00)00600-3)
5. Y. Cai, X. Lu, Q. Lin, Hollow Gaussian beams and their propagation properties, *Opt. Lett.* **28** (2003) 1084, <https://doi.org/10.1364/OL.28.001084>
6. V. V. Kotlyar, R. V. Skidanov, S. N. Khonina, V. A. Soifer,

- Hypergeometric modes, *Opt. Lett.* **32** (2007) 742, <https://doi.org/10.1364/OL.32.000742>
7. E. Karimi, G. Zito, B. Piccirillo, L. Marrucci, E. Santamato, Hypergeometric-Gaussian modes, *Opt. Lett.* **32** (2007) 3053, <https://doi.org/10.1364/OL.32.003053>
  8. V. V. Kotlyar, A. A. Kovalev, Family of hypergeometric laser beams, *J. Opt. Soc. Am. A* **25** (2008) 262, <https://doi.org/10.1364/JOSAA.25.000262>
  9. M. A. Bandres, J. C. Gutiérrez-Vega, Circular beams, *Opt. Lett.* **33** (2008) 177, <https://doi.org/10.1364/OL.33.000177>
  10. D. Stoler, Operator methods in physical optics, *J. Opt. Soc. Am.* **71** (1981) 334, <https://doi.org/10.1364/JOSA.71.000334>
  11. V. Arrizón, U. Ruiz, R. Carrada, L. A. González, Pixelated phase computer holograms for the accurate encoding of scalar complex fields, *J. Opt. Soc. Am. A* **24** (2007) 3500, <https://doi.org/10.1364/JOSAA.24.003500>
  12. H. M. Moya-Cessa *et al.*, Cauchy-Riemann beams, *Phys. Rev. A* **109** (2024) 043528, <https://doi.org/10.1103/PhysRevA.109.043528>
  13. I. Ramos-Prieto, D. Sánchez-de-la-Llave, U. Ruíz, V. Arrizón, F. Soto-Eguibar, and H. M. Moya-Cessa, Cauchy-Riemann beams in GRIN media, *Optik* **309** (2024) 171864, <https://doi.org/10.1016/j.ijleo.2024.171864>.
  14. M. Abramowitz, I. A. Stegun, and R. H. Romer, Handbook of mathematical functions with formulas, graphs, and mathematical tables (American Association of Physics Teachers, 1988).
  15. F. W. Olver, D. W. Lozier, R. F. Boisvert, C. W. Clark, NIST Handbook of Mathematical Functions, (Cambridge University Press, 2010).
  16. I. S. Gradshteyn, I. M. Ryzhik, Table of integrals, series, and products, (Academic press, 2014).